Heat Transfer Analysis using Finite Element Method under Convective Boundary Condition

Sheetal Gonsalvesa[1]*, *Swapnaa* G[1]

[1]Department of Basic Science & Humanities, MPSTME, SVKM's NMIMS, Mumbai-56, Maharashtra, India

Abstract. The model in this study scrutinizes the effect of convective boundary conditions on the flow of a nanofluid across permeable flat plate. The fundamental equations get altered into a nonlinear form through choosing appropriate similarity transformations. In the process, they are solved mathematically by substantiated FEM code through use of variational finite element method. The outcomes clearly show the characteristics of relevant parameters such as temperature and velocity profiles. When the numerical analysis is evaluated in context of formerly published information, the reliability of the numerical code is conformed. Its found that there is a surge in thermal conductivity when proportion of nanoparticles rises in the fluid. Permeability of plate has a significant influence on the heat transfer and skin friction. The investigation supports the possibility of extending the work to flows of non-Newtonian fluid, three dimensional and for consideration of pressure gradients on arbitrary surfaces. The results practically aid the design of heat transfer systems for futuristic technology involving heat enhancement.

1. Introduction

In the past decade, nanotechnology has gained significant attention in many engineering areas. Effective techniques for fluid cooling and heating are needed in numerous areas like power, transportation, manufacturing, and electronic devices. Choi [1] proposed the term nanofluid for the fluid containing nanometre sized (1-100 nm) particles known as nanoparticles. Masuda et al. [2] first studied the thermal conductivity enhancement using nanofluid. Nanoparticle size influence the transport capabilities of the fluid. The thermal characteristics of nanofluid were enhanced by maintaining minimum nanoparticle 5% volume fraction [3, 4].

*Corresponding author: Sheetal.gonsalves@nmims.edu

Nanofluids have potential applications in space technology [5], biomedical [6,7], material processing [8], solar devices [9] and combustion processes [10,11]. Recently Assael MJ et al. [12] presented several potential applications of nanofluids for heat transfer. In industrial applications such as chemical coating of vertical flat plates, hot rolling, wire drawing, etc., boundary layer flows past flat bodies are regularly encountered [13]. Stokes [14, 15] first studied the viscous incompressible flow over horizontal flat plate. Soundalgekar et al. [16] examined corresponding problem for vertical plate. Siegal [17] conducted the initial investigations over vertical plate. These results correspond with the experiments of Goldstein and Eckert [18]. A momentous volume of research on flow over flat plate has been testified [19-27]. Recently, Zainal et al. [28] investigated stagnation point, mixed convection flow past flat plate, Klazly and Bognar [29] examined the nanofluid flow using CFD simulations, Singh et al. [30] used technique of quasi-linearization to study viscous dissipation over plate, K. Mair et al. [31] has presented study based on entropy generation for Blasisus flow.

In various engineering problems, the process of suction/injection is important in context of surface heat transfer characteristics applicable in chemical and mechanical design [32-35]. heat exchange is dominant in many critical industrial processes. Swapna et al. [36] presented their work for the impact of convective boundary conditions. Many studies considering convective heat transfer for different geometries are reported [37-42]. To investigate the behavior of nanofluids considering the solid volume fraction, the model developed by Tiwari and Das [43] has been widely used in literature [44-46].

The present work thus examines the heat transfer flow taking into account convective boundary surface condition and solid volume fraction over permeable flat plate employing finite element method. Highly efficient, robust, extensively validated, novel FEM code is applied here. This study adds to engineering science literature of computational multiphysical nanofluid dynamics simulation.

2. Model Formulation

Consider 2D, steady, laminar, incompressible nanofluid flow over permeable semi-infinite flat plate. We get coefficient of heat transfer h_f by heating left side of the plate through convection from a hot fluid at temperature T_f, T_∞ is the temperature of nanofluid. The velocity of the far flow from the plate is U_∞ and mass flux velocity S_w is presumed to be constant. The flow geometry is shown in **Fig. 1.**

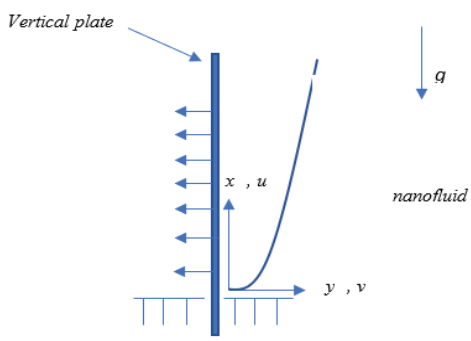

Fig.1. Flow geometry.

Further, assuming valid Boussinesq and boundary layer approximations. Since flow is over a flat surface and hence the pressure gradient is zero, the basic steady equations following the work [47] are:

$$\frac{\partial u_1}{\partial x_1}+\frac{\partial v_1}{\partial y_1}=0 \tag{1}$$

$$u_1\frac{\partial u_1}{\partial x_1}+v_1\frac{\partial u_1}{\partial y_1}=\nu_{nf}\frac{\partial^2 u_1}{\partial y_1^{\,2}} \tag{1}$$

$$u_1\frac{\partial T_1}{\partial x_1}+v_1\frac{\partial T_1}{\partial y_1}=\frac{k_{nf}}{\left(\rho C_p\right)_{nf}}\left(\frac{\partial^2 T_1}{\partial y_1^{\,2}}\right) \tag{2}$$

subject to velocity field boundary conditions:

$$\begin{aligned} &u_1=0, v_1=S_w\left(x_1\right) \text{ when } y_1=0\\ &u_1\to U_\infty \text{ as } y_1\to\infty \end{aligned} \tag{3}$$

where $S_w\left(x_1\right)$ is the injection, suction velocity when $S_w\left(x_1\right)>0$, $S_w\left(x_1\right)<0$ and $S_w\left(x_1\right)=0$ for an impermeable plate.

Thermal field boundary conditions are:

$$\begin{aligned} &y_1=0: -k_{nf}\frac{\partial T_1}{\partial y_1}=h_f\left[T_f-T_1\right]\\ &y_1\to\infty: T_1\to T_\infty \end{aligned} \tag{4}$$

Generally, $\Psi_1\left(x_1,y_1\right)$ (stream function) is defined as $u_1=\frac{\partial\Psi_1}{\partial y_1}$, $v_1=-\frac{\partial\Psi_1}{\partial x_1}$ so that it satisfies equation **Error! Reference source not found.**.

Further, introducing nondimensional similarity variables:

$$f_1\left(\eta_1\right)=\frac{\Psi_1\left(x_1,y_1\right)}{\sqrt{U_\infty\nu_f x_1}},\quad \eta_1=y_1\sqrt{\frac{U_\infty}{\nu_f x_1}},\quad \theta_1\left(\eta_1\right)=\frac{T_1-T_\infty}{T_f-T_\infty} \tag{5}$$

From equation (5) we get:

$$\Psi_1\left(x_1,y_1\right)=\sqrt{U_\infty\nu_f x_1}\,.f_1\left(\eta_1\right) \tag{6}$$

Therefore

$$\begin{aligned} &u_1=U_\infty f_1'\left(\eta_1\right)\\ &v_1=\frac{1}{2}\left(\frac{U_\infty\nu_f}{x_1}\right)^{1/2}\left(\eta_1 f_1'\left(\eta_1\right)-f_1\left(\eta_1\right)\right) \end{aligned} \tag{7}$$

$$s_w(x_1) = -\frac{1}{2}\left(\frac{U_\infty \nu_f}{x_1}\right)^{1/2} s_w \tag{8}$$

In view of equation (5), equations (1) and (2) get transformed to non-linear ODE

$$2f_1''' + \phi_1 f_1 f_1'' = 0 \tag{9}$$

$$\theta_1'' + \frac{1}{2}\Pr\left(\frac{k_f}{k_{nf}}\right)\phi_2 f_1 \theta_1' = 0 \tag{10}$$

$$\text{Here,}\quad \phi_1 = (1-\phi)^{2.5}\left[1-\phi+\phi\left(\frac{\rho_s}{\rho_f}\right)\right],\quad \phi_2 = \left[1-\phi+\phi\frac{(\rho C_p)_s}{(\rho C_p)_f}\right] \tag{11}$$

With boundary conditions:

$$\begin{aligned} &f_1(0) = s_w,\ \theta_1'(0) = -a\left[1-\theta_1(0)\right],\ f_1'(0) = 0, \\ &f_1'(\eta_1) \to 1,\ \theta_1(\eta_1) \to 0\ \ as\ \ \eta_1 \to \infty \end{aligned} \tag{12}$$

where, $a = \frac{c}{k_{nf}}\left(\frac{\nu_f}{U_\infty}\right)^{\frac{1}{2}}$ is parameter of convective heat transfer, ϕ is solid (nanoparticle) volume fraction, $\Pr = \frac{\mu_f (C_p)_f}{k_f}$ is Prandtl number and s_w is rate of transpiration (8) at surface.

We must note, similarity solution is possible, if quantity 'a' is a constant and not a function of x_1. Thus, we get, $h_f = c\,x_1^{-1/2}$ where c is constant [39].

Here, the dynamic viscosity μ_{nf}, heat capacity $(\rho C_p)_{nf}$, thermal conductivity k_{nf} and the density ρ_{nf} of nanofluid are as follows [44, 47]:

$$\begin{aligned} &\mu_{nf} = \frac{\mu_f}{(1-\phi)^{2.5}} \\ &(\rho C_p)_{nf} = (1-\phi)(\rho C_p)_f + \phi(\rho C_p)_s \\ &\frac{k_{nf}}{k_f} = \frac{k_s + 2k_f - 2\phi(k_f - k_s)}{k_s + 2k_f + \phi(k_f - k_s)} \\ &\rho_{nf} = (1-\phi)\rho_f + \phi\rho_s \end{aligned} \tag{13}$$

The values of rate of heat transfer $-\theta_1'(0)$ and the rate of shear stress $f_1''(0)$ at the surface (the local Nusselt number, the skin friction coefficient) are of practical interest.

3. Mathematical Analysis

3.1 Finite element modelling

Details of method used here are available in the work by Reddy [50].

The finite-element modelling stages are given by,

3.1.1. Discretization of Finite-element

The entire area is alienated into a fixed number of subdomains known as an element. Finite-element mesh is obtained by assembling elements.

3.1.2. Element equations generation

i. For given problem, variational formulation is constructed by isolating a typical element from the mesh.

ii. An estimated answer of the variational problem is presumed. Using this solution in the system obtained element equations are written.

iii. The element interpolation functions are used to construct element matrix.

3.1.3. Element equations assembling

Applying continuity conditions for interelement, numerical equations are assembled. The entire domain is governed by global finite-element model constructed from these numerical equations.

3.1.4. Applying boundary conditions

The constructed equations are imposed by natural and essential boundary conditions.

3.1.5. Solving assembled equations

The numerical techniques, such as LU decomposition, Gauss elimination, etc. are used to solve assembled equations. Here, actual functions are approximated by shape functions.

To solve the non-linear ODE (9) and (10) subject to boundary conditions (12) , let first assume:

$$f_1' = h_1 \tag{14}$$

The system gets reduce to:

$$2h_1'' + \phi_1 f_1 h_1' = 0 \tag{15}$$

$$\theta_1'' + \frac{1}{2}\Pr\left(\frac{k_f}{k_{nf}}\right)\phi_2 f_1 \theta_1' = 0 \tag{16}$$

and boundary conditions become:

$$\begin{aligned} &f_1(0)=s_w, \quad h_1(0)=0, \\ &\theta_1'(0)=-a\left[1-\theta_1(0)\right], \\ &h_1(\infty)=1, \quad \theta_1(\infty)=0. \end{aligned} \tag{17}$$

3.2 Variational form

The variational form linked with equations (14)-(16) over element (η_e, η_{e+1}) is:

$$\int_{\eta_e}^{\eta_{e+1}} w_1\left(f_1' - h_1\right) d\eta_1 = 0 \tag{18}$$

$$\int_{\eta_e}^{\eta_{e+1}} w_2\left(2h_1'' + \phi_1 f_1 h_1'\right) d\eta_1 = 0 \tag{19}$$

$$\int_{\eta_e}^{\eta_{e+1}} w_3\left(\theta_1'' + \frac{1}{2}\Pr\left(\frac{k_f}{k_{nf}}\right)\phi_2 f_1 \theta_1'\right) d\eta_1 = 0 \tag{20}$$

Here, w_1, w_2, w_3 are linearly independent functions known as weight functions corresponding to the variation in the functions f_1, h_1, θ_1 respectively.

3.3 Finite element form

To obtain the finite element model, we substitute following approximations into equations (18)-(20).

$$f_1 = \sum_{j=1}^{2}(f_1)_j \psi_j \ , \ h_1 = \sum_{j=1}^{2}(h_1)_j \psi_j \ , \ \theta_1 = \sum_{j=1}^{2}(\theta_1)_j \psi_j \tag{21}$$

Here $\psi_i = w_1 = w_2 = w_3$ ($i = 1,2$),

Linear interpolation functions:

$$\psi_1 = (\eta_{e+1} - \eta_1)(\eta_{e+1} - \eta_e)^{-1} \ , \ \psi_2 = (\eta_1 - \eta_e)(\eta_{e+1} - \eta_e)^{-1} \ , \quad \eta_e \le \eta_1 \le \eta_{e+1} \tag{22}$$

Quadratic interpolation functions:

$$\begin{aligned} &\psi_1 = (\eta_{e+1} + \eta_e - 2\eta_1)(\eta_{e+1} - \eta_1)(\eta_{e+1} - \eta_e)^{-2} \ , \\ &\psi_2 = 4(\eta_1 - \eta_e)(\eta_{e+1} - \eta_1)(\eta_{e+1} - \eta_e)^{-2} \ , \\ &\psi_3 = (\eta_{e+1} + \eta_e - 2\eta_1)(\eta_1 - \eta_e)(\eta_{e+1} - \eta_e)^{-2} \ , \ \eta_e \le \eta_1 \le \eta_{e+1} \end{aligned}$$

The developed finite element model is stated as:

$$\begin{bmatrix} [K^{11}] & [K^{12}] & [K^{13}] \\ [K^{21}] & [K^{22}] & [K^{23}] \\ [K^{31}] & [K^{32}] & [K^{33}] \end{bmatrix} \begin{pmatrix} \{f_1\} \\ \{h_1\} \\ \{\theta_1\} \end{pmatrix} = \begin{pmatrix} \{r^1\} \\ \{r^2\} \\ \{r^3\} \end{pmatrix} \tag{23}$$

Here $[K^{mn}]$ are 2×2 and $\{r^m\}$ are 2×1 order matrices ($m,n=1,2,3$).

Matrices are given by:

$$K_{ij}^{11} = \int_{\eta_e}^{\eta_{e+1}} \psi_i \frac{d\psi_j}{d\eta_1} d\eta_1 \ , \ K_{ij}^{12} = -\int_{\eta_e}^{\eta_{e+1}} \psi_i \psi_j d\eta_1 \ , \ K_{ij}^{13} = 0$$

$$K_{ij}^{21} = 0, \ K_{ij}^{22} = -2\int_{\eta_e}^{\eta_{e+1}} \frac{d\psi_i}{d\eta_1}\frac{d\psi_j}{d\eta_1} d\eta_1 + (\phi_1)\int_{\eta_e}^{\eta_{e+1}} \overline{f_1}\psi_i \frac{d\psi_j}{d\eta_1} d\eta_1 \ , \ K_{ij}^{23} = 0 \tag{24}$$

$$K_{ij}^{31} = 0, \ K_{ij}^{32} = 0, \ K_{ij}^{33} = -\int_{\eta_e}^{\eta_{e+1}} \frac{d\psi_i}{d\eta_1}\frac{d\psi_j}{d\eta_1} d\eta_1 + \left(\frac{1}{2}\Pr\left(\frac{k_f}{k_{nf}}\right)\phi_2\right)\int_{\eta_e}^{\eta_{e+1}} \overline{f_1}\psi_i \frac{d\psi_j}{d\eta_1} d\eta_1$$

$$r_i^1 = 0 \ , \ r_i^2 = -\left[\psi_i \frac{dh_1}{d\eta_1}\right]_{\eta_e}^{\eta_{e+1}} \ , \ r_i^3 = -\left[\psi_i \frac{d\theta_1}{d\eta_1}\right]_{\eta_e}^{\eta_{e+1}} \tag{25}$$

with $\overline{f_1} = \sum_{i=1}^{2} \overline{(f_1)}_i \psi_i$ (26)

No significant change in the results has been observed for large values of $\eta_1 (>10)$. Thus, without loss of generality for the computational purposes, ∞ can be fixed at 10. The total domain is split into n-linear elements having width $h_e (= \eta_{e+1} - \eta_e)$ where $h_e = \frac{10}{n}$. The calculations are carried out for 200, 250, 300, 350, 400, 500 and 1000 elements and n = 400 is fixed.

The order of the element matrix (23) is 6×6. If we split domain into 400 equal linear elements, after assembling all element equations we get 1203×1203 order matrix. The system obtained is highly nonlinear and linearized by incorporating the function $\overline{f_1}$. By sustaining an accuracy of 0.0001, an iterative scheme for f_1, h_1 and θ_1 is used to solve the remaining system of non-linear equations.

The interpolation functions for 1D and 2D problems, can be linear, quadratic and higher order. Though, the fitness of the shape functions differs with the problem. Linear and quadratic shape functions are used owing to the simple and effective usage in computations. **Table 1** gives evaluation for both types of interpolation function, and observed that the outcomes do not differ much, indicating that both elements provide almost the same precision.

Table 1: Results of f_1, $\partial f_1 / \partial \eta_1$ and θ_1 for linear as well as quadratic elements when step size = 0.1, $\Pr = 6.2$, $\phi = 0.01$, $a = 0.5$, $s_w = 1$.

η_1	f_1		$\partial f_1 / \partial \eta_1$		θ_1	
	Quadratic	Linear	Quadratic	Linear	Quadratic	Linear
0.0	1.0000	1.0000	0.0000	0.0000	0.1357	0.1357
0.4	1.0546	1.0546	0.2641	0.2641	0.0355	0.0355
1.0	1.3093	1.3093	0.5671	0.5671	0.0033	0.0033
1.4	1.5668	1.5668	0.7135	0.7135	0.0005	0.0005
2.0	2.0431	2.0431	0.8611	0.8611	0.0000	0.0000

4. Code Validation

To evaluate the accuracy and the efficiency of the FEM code, the numerical results of $-\theta_1'(0)$ for values of *a* and numerical values of f_1, $(f_1)'$ and $(f_1)''$ with variation in η_1 are depicted in **Table 2 and 3** respectively. The results are in good correlation with previous studies, testifying to the validity of the code. In order to further validate the trends of temperature and velocity profiles, for various values of ϕ the developed temperature profiles have been graphically shown in **Fig. 2** and they are depicting the same trend as those analysed previously by Anjali Devi and Julie Andrews [47]. Further, profiles of the temperature and velocity for s_w are graphically depicted in **Fig. 3** and **Fig. 4** and the trends are qualitatively similar with those of Ishak [38]. Thus, it confirms the authenticity of our numerical code.

Table 2: Results for $-\theta_1'(0)$ by varying *a* when $\phi = 0$, $s_w = 0$, $\Pr = 0.1$.

a	**Aziz [37]**	**Ishak [38]**	**Present result**
0.1	0.0594	0.058338	0.058338
0.2	0.0848	0.082363	0.082346
0.4	0.1076	0.103720	0.103693
0.6	0.1182	0.113533	0.113501
0.8	0.1243	0.119170	0.119135
1	0.1283	0.122830	0.122792
5	0.1430	0.136215	0.136169
10	0.1450	0.138096	0.138049
20	0.1461	0.139056	0.139008

Table 3: Results for f_1, $(f_1)'$, $(f_1)''$ by varying η when $\phi = 0$, $s_w = 0$

η_1	**Howarth [49]**			**Cortell [48]**			**Present result**		
	f_1	$(f_1)'$	$(f_1)''$	f_1	$(f_1)'$	$(f_1)''$	f_1	$(f_1)'$	$(f_1)''$
0	0.00000	0.00000	0.33206	0.00000	0.00000	0.33206	0.00000	0.00000	0.33206
1	0.16557	0.32978	0.32301	0.16557	0.32978	0.32301	0.16557	0.32978	0.32301
2	0.65003	0.62977	0.26675	0.65003	0.62977	0.26675	0.65003	0.62977	0.26675
3	1.39682	0.84605	0.16136	1.39682	0.84605	0.16136	1.39682	0.84605	0.16136
4	2.30576	0.95552	0.06423	2.30576	0.95552	0.06423	2.30576	0.95552	0.06423
5	3.28330	0.99155	0.01591	3.28330	0.99155	0.01591	3.28330	0.99155	0.01591
6	4.27965	0.99898	0.00240	4.27965	0.99898	0.00240	4.27965	0.99898	0.00240
7	5.27927	0.99993	0.00022	5.27927	0.99993	0.00022	5.27927	0.99993	0.00022
8	6.27925	1.00000	0.00001	6.27925	1.00000	0.00001	6.27925	1.00000	0.00001
9	7.27925	1.00000	0.00000	7.27925	1.00000	0.00000	7.27925	1.00000	0.00000

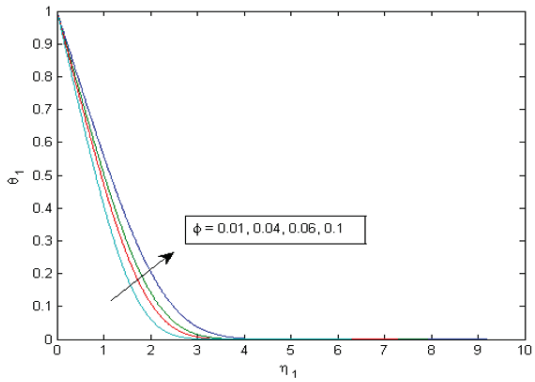

Fig. 2. Variation in temperature profiles $\theta_1(\eta_1)$ with ϕ, $f_w = 0$, $\Pr = 6.2$, n=1000.

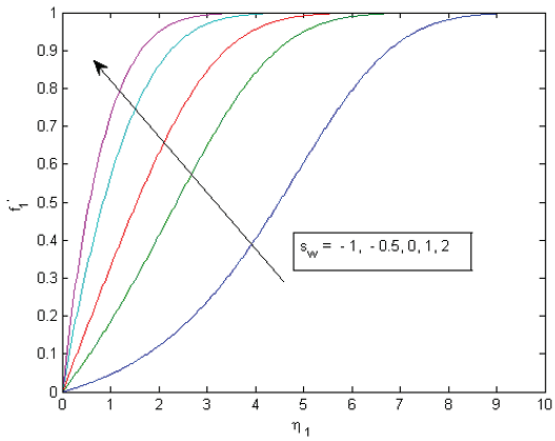

Fig. 3. Variation in Velocity profiles $f_1'(\eta_1)$ with s_w, $\phi = 0$, $a = 1$, $\Pr = 1$.

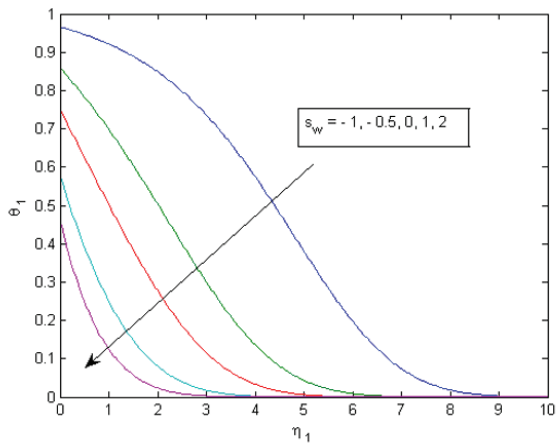

Fig. 4. Variation in Temperature profiles $\theta_1(\eta_1)$ with s_w, $\Pr = 1, a = 1, \phi = 0$.

5. Results and Discussion

Impact on the temperature and velocity distributions with variation in thermophysical parameters i.e. ϕ, s_w, and a are shown in **Fig. 5-8**. The numerical results for the skin friction coefficient $f_1''(0)$ and rate of heat transfer $-\theta_1'(0)$ are reported in **Table 4** and **Table 5** for selected parameters.

In **Fig. 5**, it is observed that, the temperature increases if volume fraction is increased. Owing to the high thermal conductivity of the CuH_2O nanofluid and further with increase in volume fraction, the resistance between the nanofluid and the wall becomes high which tends to rise thickness of thermal boundary layer.

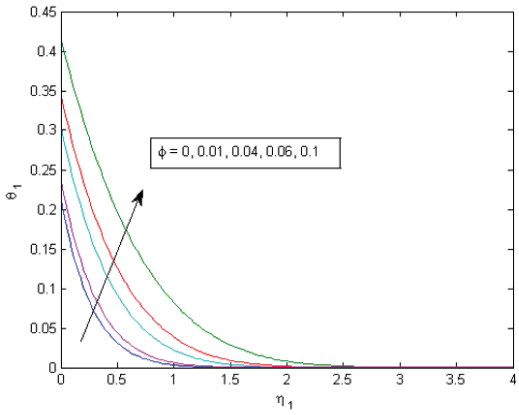

Fig. 5. Impact of ϕ on temperature profiles $\theta_1(\eta_1)$, $a=1$, $\Pr=6.2$, $f_w=1$.

Fig. 6, 7 exhibit the evolution of velocity and temperature for the effect of injection/suction, respectively. It is observed from **Fig. 6**, as suction ($s_w>0$) increases, the velocity also increases. It is also noted that the flow is strongly decelerated with suction $s_w=2$, while it is accelerated with increasing injection $s_w=-0.5$. This is because suction causes the boundary layer to cling more firmly to the plate, thereby decreasing the momentum boundary layer thickness. Conversely, injection assists in momentum development as more nanofluid particles are added through the plate thereby enhancing the velocity and increasing the thickness of momentum boundary layer. It is distinctly observed from **Fig. 7** that the temperature decreases with increasing suction. On the other hand, injection or blowing is found to enhance the temperature.

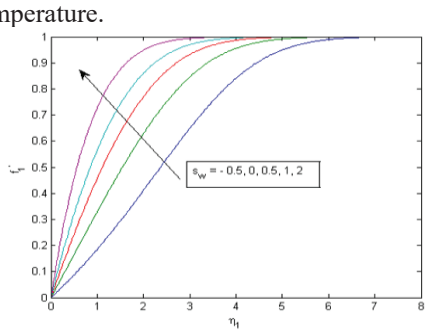

Fig. 6. Impact of s_w on velocity profiles $f_1'(\eta_1)$, $\phi=0.01$, $\Pr=6.2$, $a=1$.

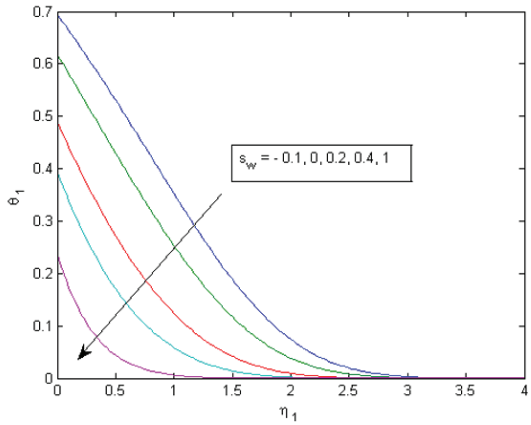

Fig. 7. Impact of s_w on temperature profiles $\theta_1(\eta_1)$, $\phi = 0.01$, $\Pr = 6.2$, $a = 1$.

In **Fig. 8,** relation between a and θ_1 is depicted. It is observed that as convective heat transfer parameter increases, surface temperature $\theta_1(0)$ increases. This is due to the hot fluid side thermal resistance and h_f are inversely proportional to each other. Further, it is seen from the figure that $\theta_1(0) = 1$ as $a \to \infty$. It can be observed from equation (9) that a has no effect on the flow field.

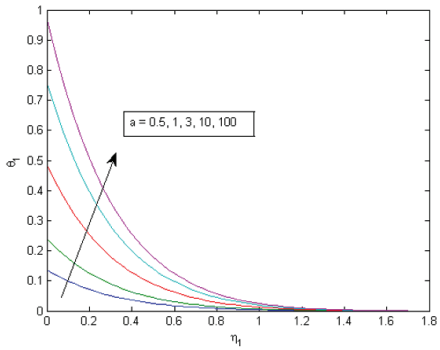

Fig. 8. Impact of a on Temperature profiles $\theta_1(\eta_1)$, $s_w = 1$, $\Pr = 6.2$, $\phi = 0.01$.

The impact of suction/injection and convective heat transfer parameter has been calculated on the $f_1''(0)$, $-\theta_1'(0)$ and depicted in **Table 4** and **Table 5**, respectively. It is noted from **Table 4** that $f_1''(0)$ increases with increasing s_w. The surface shear stress is more for suction ($s_w > 0$) in contrast to injection ($s_w < 0$). It is also detected the heat transfer rate at the surface $-\theta_1'(0)$ is higher for the suction. This phenomenon is due to introduction of suction causing rise in surface shear stress along with surge in local Nusselt number. It is noted from **Table 5** that heat transfer rate is boosted as a increases. Further, the plate high inner thermal resistance is due to higher value of the convective parameter.

Table 4: Influence of s_w on $f_1''(0)$, $-\theta_1'(0)$ when $\phi = 0.01$, $a = 1$.

s_w	$f_1''(0)$	$-\theta_1'(0)$
-1.5	0.0008	0.0000
-1	0.0356	0.0000
-0.5	0.1645	0.0440
-0.1	0.2964	0.3052
0	0.3321	0.3809
0.1	0.3687	0.4495
0.3	0.4443	0.5608
0.5	0.5228	0.6413
1	0.7289	0.7600
2	1.1693	0.8556
3	1.6317	0.8920

Table 5: Influence of a on $-\theta_1'(0)$ when $\phi = 0.01$, $s_w = 1$.

a	$-\theta_1'(0)$
0	0
0.05	0.0492
0.1	0.0968
0.5	0.4316
1	0.7600
3	1.5428
10	2.4124
20	2.7439

6. Conclusions

A mathematical study for heat transfer of a nanofluid flow over flat plate in the presence of suction/injection with a convective surface boundary condition has been conducted. The altered system is solved by using a valid variational FEM demonstrating agreement with previous studies. The present solutions reveal that:

- Surge in the nanoparticles enhances CuH_2O nanofluid thermal conductivity.
- Increasing suction retards the nanofluid flow and decreases the temperature, whereas injection parameter does contrary.
- Heat transfer and skin friction are sturdily influenced by the suction/injection.
- The temperature, heat transfer are boosted with an increase in the convective boundary parameter
- Vigorous cooling of vertical plate may be effectively attained by judiciously implementing the parameters studied in this paper.
- The current study can be extended to flows considering pressure gradients on arbitrary surfaces and also to cases of three-dimensional flows, non-Newtonian flows.
- These findings are of practical importance in designing heat transfer systems that employ nano-fluids as their principal heat exchange medium.

Nomenclature

x_1, y_1 : Cartesian coordinates along the plate and normal to it

T_1 : temperature of fluid in boundary layer

ν_{nf} : kinematic viscosity

f_1 : dimensionless velocity

η_1 : dimensionless coordinate

θ_1 : dimensionless temperature

μ_f : viscosity of a base fluid

k_s, k_f : thermal conductivities of the solid fractions and of the fluid

ρ_s, ρ_f : densities of the solid fractions and of the fluid

Superscript

$'$: differentiation with respect to η_1

References

1. Choi, S. U. S., Singer, D. A., & Wang, H. P.: Developments and applications of non-Newtonian flows, Asme Fed, **66**, (1995), 99-105.
2. Masuda, H., Ebata, A., & Teramae, K.: Alteration of thermal conductivity and viscosity of liquid by dispersing ultra-fine particles, Dispersion of Al2O3, SiO2 and TiO2 ultra-fine particles, (1993), 227-233.
3. Godson, L., Raja, B., Lal, D. M., & Wongwises, S. E. A.: Enhancement of heat transfer using nanofluids—an overview, Renewable and sustainable energy reviews, **14**(2), (2010), 629-641.
4. Yu, W., France, D. M., Routbort, J. L., & Choi, S. U.: Review and comparison of nanofluid thermal conductivity and heat transfer enhancements, Heat transfer engineering, **29**(5), (2008), 432-460.
5. Ungar, E., & Erickson, L.: *Assessment of the use of nanofluids in spacecraft active thermal control systems*, In AIAA SPACE (2011) Conference & Exposition (p. 7328).
6. Bég, O. A., & Tripathi, D.: Mathematica simulation of peristaltic pumping with double-diffusive convection in nanofluids: a bio-nano-engineering model, Proceedings of the Institution of Mechanical Engineers, Part N: Journal of Nanoengineering and Nanosystems, **225**(3), (2011), 99-114.
7. Bég, T. A., Rashidi, M. M., Bég, O. A., & Rahimzadeh, N.: Differential transform semi-numerical analysis of biofluid-particle suspension flow and heat transfer in non-Darcian porous media, Computer methods in biomechanics and biomedical engineering, **16**(8), (2013), 896-907.
8. Chang, H., & Chang, Y. C. : Fabrication of Al2O3 nanofluid by a plasma arc nanoparticles synthesis system, Journal of Materials Processing Technology, **207**(1-3), (2008), 193-199.
9. Sani, E., Barison, S., Pagura, C., Mercatelli, L., Sansoni, P., Fontani, D., ... & Francini, F. : Carbon nanohorns-based nanofluids as direct sunlight absorbers, Optics Express, **18**(5), (2010), 5179-5187.
10. Van Devener, B., & Anderson, S. L.: Breakdown and combustion of JP-10 fuel catalyzed by nanoparticulate CeO2 and Fe2O3, Energy & Fuels, **20**(5), (2006), 1886-1894.

11. Allen, C., Mittal, G., Sung, C. J., Toulson, E., & Lee, T.: An aerosol rapid compression machine for studying energetic-nanoparticle-enhanced combustion of liquid fuels, Proceedings of the Combustion Institute, **33**(2), (2011), 3367-3374.
12. Assael, M. J., Antoniadis, K. D., Wakeham, W. A., & Zhang, X.: Potential applications of nanofluids for heat transfer, International Journal of Heat and Mass Transfer, **138**, (2019), 597-607.
13. Vaszi, A. Z., Elliott, L., Ingham, D. B., & Pop, I.: Conjugate free convection above a heated finite horizontal flat plate embedded in a porous medium, International journal of heat and mass transfer, **45**(13), (2002), 2777-2795.
14. Stokes, V. K.: Couple stresses in fluids, In Theories of Fluids with Microstructure, Springer, Berlin, Heidelberg, (1984), 34-80.
15. Stokes, V. K., Theories of fluids with microstructure, Springer, New York, (1984).
16. Soundalgekar, V. M.: Free convection effects on the Stokes problem for an infinite vertical plate, Asme, (1977), 499-501.
17. Siegel, R.: Transient free convection from a vertical flat plate, Trans. Asme, **80**(2), (1958), 347.
18. Goldstein, R. J., & Eckert, E. R. G.: The steady and transient free convection boundary layer on a uniformly heated vertical plate, International Journal of Heat and Mass Transfer, **1**(2-3), (1960), 208-218.
19. Rana, P., & Bhargava, R.: Numerical study of heat transfer enhancement in mixed convection flow along a vertical plate with heat source/sink utilizing nanofluids, Communications in Nonlinear Science and Numerical Simulation, **16**(11), 2011, 4318-4334.
20. Kuznetsov, A. V., & Nield, D. A.: The Cheng–Minkowycz problem for natural convective boundary layer flow in a porous medium saturated by a nanofluid: a revised model, International Journal of Heat and Mass Transfer, **65**, (2013), 682-685.
21. Aziz, A., & Khan, W. A.: Natural convective boundary layer flow of a nanofluid past a convectively heated vertical plate, International Journal of Thermal Sciences, 52, 2012, 83-90.
22. Turkyilmazoglu, M., & Pop, I.: Heat and mass transfer of unsteady natural convection flow of some nanofluids past a vertical infinite flat plate with radiation effect, International Journal of Heat and Mass Transfer, **59**, (2013), 167-171.
23. Makinde, O. D.: Effects of viscous dissipation and Newtonian heating on boundary-layer flow of nanofluids over a flat plate, International Journal of Numerical Methods for Heat & Fluid Flow,(2013).
24. Loganathan, P., Chand, P. N., & Ganesan, P.: Transient natural convective flow of a nanofluid past a vertical plate in the presence of heat generation, Journal of Applied Mechanics and Technical Physics, **56**(3), (2015), 433-442.
25. Vemula, R., Chamkha, A. J., & Mallesh, M. P.: Nanofluid flow past an impulsively started vertical plate with variable surface temperature, International Journal of Numerical Methods for Heat & Fluid Flow, (2016).
26. Othman MI, Mahdy AM : Numerical studies for solving a free convection boundary–layer flow over a vertical plate, Mechanics and Mechanical Engineering, **22**(1), (2018), 41-8.
27. S. Saranya, P. Ragupathi, B. Ganga, R.P. Sharma, A.K. Abdul: Hakeem,Non-linear radiation effects on magnetic/non-magnetic nanoparticles with different base fluids over a flat plate, Advanced Powder Technology, **29**(9), (2018), 1977-1990.
28. Zainal, N. A., Nazar, R., Naganthran, K., & Pop, I.: MHD mixed convection stagnation point flow of a hybrid nanofluid past a vertical flat plate with convective boundary condition, Chinese Journal of Physics, **66**, (2020), 630-644.

29. Klazly, M. M., & Bognár, G.: CFD study for the flow behaviour of nanofluid flow over flat plate, INTERNATIONAL JOURNAL OF MECHANICS, **14**,(2020), 49-57.
30. Singh, A. K., Iyyappan, G., & Jaganathan, B.: Effect of Viscous Dissipation of Laminar Flow over a Flat Plate with Variable Properties, Advances in Fluid Dynamics, (2021), 619-626.
31. Mair Khan, T. Salahuddin, Mohamed Altanji: A viscously dissipated Blasisus boundary layer flow with variable thermo-physical properties: An entropy generation study, International Communications in Heat and Mass Transfer, **131**,(2022), 105873.
32. Watanabe, T.: Forced and free mixed convection boundary layer flow with uniform suction or injection on a vertical flat plate, Acta Mechanica, **89**(1), (1991), 123-132.
33. Char, M. I.: Heat transfer of a continuous, stretching surface with suction or blowing, Journal of Mathematical Analysis and Applications, **135**(2), (1988), 568-580.
34. Bachok, N., Ishak, A., & Pop, I.: Boundary layer flow over a moving surface in a nanofluid with suction or injection, Acta Mechanica Sinica, **28**(1), (2012), 34-40.
35. Palanichamy, P.: Blasius Flow with Suction and Blowing, Global Journal of Pure and Applied Mathematics, **13**(7), (2017), 2825-2835.
36. Swapna, G., Kumar, L., Rana, P., Kumari, A., & Singh, B.: Finite element study of radiative double-diffusive mixed convection magneto-micropolar flow in a porous medium with chemical reaction and convective condition, Alexandria engineering journal, **57**(1) , (2018), 107-120.
37. Aziz, A.: A similarity solution for laminar thermal boundary layer over a flat plate with a convective surface boundary condition, Communications in Nonlinear Science and Numerical Simulation, **14**(4), (2009), 1064-1068.
38. Ishak, A.: Similarity solutions for flow and heat transfer over a permeable surface with convective boundary condition, Applied Mathematics and Computation, **217**(2), (2010), 837-842.
39. Makinde, O. D., & Aziz, A.: MHD mixed convection from a vertical plate embedded in a porous medium with a convective boundary condition, International Journal of Thermal Sciences, **49**(9), (2010), 1813-1820.
40. Rashad, A. M., Chamkha, A. J., & Modather, M.: Mixed convection boundary-layer flow past a horizontal circular cylinder embedded in a porous medium filled with a nanofluid under convective boundary condition, Computers & Fluids, **86**, (2013), 380-388.
41. Ahmad, R., & Khan, W. A.: Numerical study of heat and mass transfer MHD viscous flow over a moving wedge in the presence of viscous dissipation and heat source/sink with convective boundary condition, Heat Transfer—Asian Research, **43**(1), (2014), 17-38.
42. Jha BK, Samaila G.: Thermal radiation effect on boundary layer over a flat plate having convective surface boundary condition, SN Applied Sciences, **2**(3), (2020), 1-8.
43. Tiwari, R. K., & Das, M. K.: Heat transfer augmentation in a two-sided lid-driven differentially heated square cavity utilizing nanofluids, International Journal of heat and Mass transfer, **50**(9-10),(2007), 2002-2018.
44. Oztop, H. F., & Abu-Nada, E.: Numerical study of natural convection in partially heated rectangular enclosures filled with nanofluids, International journal of heat and fluid flow, **29**(5), (2008), 1326-1336.
45. Ahmad, M. J., & Tiwari, G. N.: Solar radiation models—A review, International Journal of Energy Research, **35**(4), (2011), 271-290.
46. Yacob, N. A., Ishak, A., & Pop, I.: Falkner–Skan problem for a static or moving wedge in nanofluids, International Journal of Thermal Sciences, **50**(2), (2011), 133-139.
47. Devi, S. A., & Andrews, J.: Laminar boundary layer flow of nanofluid over a flat plate, Int. J. Appl. Math. Mech, **7**(6), (2011), 52-71.

48. Cortell, R.: Numerical solutions of the classical Blasius flat-plate problem, Applied Mathematics and Computation, **170**(1), (2005), 706-710.
49. Howarth, L.: On the solution of the laminar boundary layer equations, Proceedings of the Royal Society of London. Series A-Mathematical and Physical Sciences, **164**(919), (1938), 547-579.
50. Reddy, J. N., Introduction to the finite element method, McGraw-Hill Education, (2019).